Simulation of climate response to aerosol direct and indirect effects with aerosol transport-radiation model

Toshihiko Takemura,[1] Toru Nozawa,[2] Seita Emori,[2] Takashi Y. Nakajima,[3] and Teruyuki Nakajima[4]

Received 18 May 2004; revised 7 October 2004; accepted 12 November 2004; published 22 January 2005.

[1] With a global aerosol transport-radiation model coupled to a general circulation model, changes in the meteorological parameters of clouds, precipitation, and temperature caused by the direct and indirect effects of aerosols are simulated, and its radiative forcing are calculated. A microphysical parameterization diagnosing the cloud droplet number concentration based on the Köhler theory is introduced into the model, which depends not only on the aerosol particle number concentration but also on the updraft velocity, size distributions, and chemical properties of each aerosol species and saturation condition of the water vapor. The simulated cloud droplet effective radius, cloud radiative forcing, and precipitation rate, which relate to the aerosol indirect effect, are in reasonable agreement with satellite observations. The model results indicate that a decrease in the cloud droplet effective radius by anthropogenic aerosols occurs globally, while changes in the cloud water and precipitation are strongly affected by a variation of the dynamical hydrological cycle with a temperature change by the aerosol direct and first indirect effects rather than the second indirect effect itself. However, the cloud water can increase and the precipitation can simultaneously decrease in regions where a large amount of anthropogenic aerosols and cloud water exist, which is a strong signal of the second indirect effect. The global mean radiative forcings of the direct and indirect effects at the tropopause by anthropogenic aerosols are calculated to be -0.1 and -0.9 W m^{-2}, respectively. It is suggested that aerosol particles approximately reduce 40% of the increase in the surface air temperature by anthropogenic greenhouse gases on the global mean.

Citation: Takemura, T., T. Nozawa, S. Emori, T. Y. Nakajima, and T. Nakajima (2005), Simulation of climate response to aerosol direct and indirect effects with aerosol transport-radiation model, *J. Geophys. Res.*, *110*, D02202, doi:10.1029/2004JD005029.

1. Introduction

[2] Aerosol particles are considered to be one of the factors inducing climate change mainly through two effects. One is a direct effect in which aerosol particles scatter and absorb the solar and thermal radiation. The other is an indirect effect in which they change the microphysical and optical properties of cloud droplets acting as cloud condensation nuclei (CCN). The indirect effect can be, moreover, divided into two categories. The first indirect effect is that the cloud droplet effective radius decreases if the aerosol particle number concentration increases, leading to the higher cloud albedo [*Twomey*, 1974]. The second one is that a decrease in the cloud droplet effective radius also results in an inhibition of precipitation and an increase in the cloud water [*Albrecht*, 1989].

[3] The Third Assessment Report (TAR) of the Intergovernmental Panel on Climate Change (IPCC) [*Intergovernmental Panel on Climate Change* (*IPCC*), 2001] estimated that the radiative forcing due to anthropogenic aerosols is -0.5 W m^{-2} with an uncertainty factor of 2 for the direct effect and from 0 to -2.0 W m^{-2} without a plausible value for the first indirect effect. The second indirect effect could not be estimated because of a much lower confidence. These results indicate that there is a larger uncertainty in the evaluation of the aerosol radiative forcing, especially of the indirect effect, than of the greenhouse gases which exist more homogeneously than aerosol particles both spatially and temporally. The *IPCC* [2001] mainly compiled past modeling studies on estimating the aerosol radiative forcing, while *Nakajima et al.* [2001] derived the indirect radiative forcing to be from -0.7 to -1.7 W m^{-2} based on retrieved data from the advanced very high resolution radiometer (AVHRR) loaded on the National Oceanic and Atmospheric Administration satellite. *Lohmann and Lesins* [2002] constrained the model-estimated indirect radiative forcing with the relationship between the satellite-derived cloud effective radius, cloud

[1]Research Institute for Applied Mechanics, Kyushu University, Fukuoka, Japan.
[2]National Institute for Environmental Studies, Ibaraki, Japan.
[3]Earth Observation Research Center, Japan Aerospace Exploration Agency, Tokyo, Japan.
[4]Center for Climate System Research, University of Tokyo, Tokyo, Japan.

0148-0227/05/2004JD005029$09.00

water path, and aerosol loading from the Polarization and Directionality of the Earth's Reflectances (POLDER), so that it was reduced from -1.4 to -0.85 W m^{-2}. The information on cloud properties, such as the effective radius and liquid water path, acquired from satellites is useful for reducing the uncertainty of the aerosol indirect effect.

[4] Modeling studies about aerosol effects on climate change are progressing in which changes in the primary meteorological parameters, such as wind, temperature, cloud water, and precipitation, due to anthropogenic and natural aerosols are quantitatively estimated in order to analyze the past climate in detail and to improve the confidence level for predicting future climates. *Miller and Tegen* [1998] simulated the climate response to the direct effect of soil dust aerosols with an atmospheric general circulation model (AGCM) including a mixed layer ocean model for discussing changes in the heat flux, precipitation, and surface temperature. *Rotstayn and Lohmann* [2002] studied a change in the precipitation by the first and second indirect effects of anthropogenic sulfate aerosols using an AGCM coupled with a mixed layer ocean and indicated a southward shift in tropical rainfall in response to the aerosol indirect effect. Simple formulae only with the aerosol mass concentration were, however, used for diagnosing the cloud droplet number concentration in order to estimate the aerosol indirect effect in most past studies. It is also necessary to carry out a comprehensive simulation for analyzing climate response to the aerosol effects including all of the main tropospheric aerosols to improve the accuracy of reproducing the past climate and predicting the future climate changes.

[5] In this study, a global aerosol transport-radiation model, Spectral Radiation-Transport Model for Aerosol Species (SPRINTARS) [*Takemura et al.*, 2000, 2002a] simulates changes in the meteorological field due to the aerosol direct and indirect effects. It is completely coupled with an atmospheric general circulation model including a mixed layer ocean, and it treats the main tropospheric aerosols. The cloud droplet number concentration is diagnosed by a parameterization considering the cloud microphysical processes based on the Köhler theory, which includes not only the aerosol particle number concentration but also the updraft velocity, size distributions and chemical properties of each aerosol species, and saturation condition of the water vapor. We especially focus on differences in the simulated cloud droplet effective radius, cloud water path, precipitation, and temperature between the preindustrial era and the present day. The model description is given in section 2. Section 3 shows the global distributions of the simulated cloud parameters and precipitation considering the aerosol effects, compares them with several observations, and discusses the aerosol direct and indirect radiative forcing. Changes in the cloud, precipitation, and temperature due to anthropogenic aerosols are discussed in section 4. Our conclusions are then presented in section 5.

2. Model Description

[6] The global three-dimensional aerosol transport-radiation model, SPRINTARS, is driven by the AGCM jointly owned by the Center for Climate System Research (CCSR)/University of Tokyo, National Institute for Environmental Studies (NIES), and Frontier Research Center for Global Change (FRCGC) [*Numaguti et al.*, 1995]. The model predicts mass mixing ratios of the main tropospheric aerosols, that is, carbonaceous (black carbon (BC) and organic carbon (OC)), sulfate, soil dust, and sea salt, and the precursor gases of sulfate, that is, sulfur dioxide (SO_2) and dimethylsulfide (DMS). The aerosol transport processes include emission, advection, diffusion, sulfur chemistry, wet deposition, and gravitational settling. The radiation scheme in CCSR/NIES/FRCGC AGCM [*Nakajima et al.*, 2000] is extended for the aerosol direct effect related to scattering and absorption by aerosol particles. The detailed description of SPRINTARS is given by *Takemura et al.* [2000, 2002a].

[7] Time series of the emission fluxes for anthropogenic aerosols and their precursors from 1850 to 2000 are provided by our research group (T. Nozawa et al., personal communication, 2004). Figure 1 shows the global distributions of annual mean emissions of BC, OC, and SO_2 in 2000 and their global annual total emissions both in 1850 and 2000 are in Table 1. The emissions of carbonaceous aerosols originating from biomass burning, biofuel, agricultural activity, and fossil fuels are based on several databases from the Food and Agriculture Organization of the United Nations (FAO), Global Emissions Inventory Activities (GEIA), and energy statistics in each nation. That of fossil fuel SO_2 refers to the A.S.L & Associates database. The History Database of the Global Environment (HYDE) is used for population changes and land use. The volcanic SO_2 from continuous eruptions refers to the GEIA database, and biomass burning SO_2 is based on the GEIA database and *Spiro et al.* [1992]. The monthly mean oxide field of OH, H_2O_2, and O_3 for the sulfur chemistry is prescribed by the global chemical model, CHASER, which is driven by the CCSR/NIES/FRCGC AGCM [*Sudo et al.*, 2002] using the same historical emission database as SPRINTARS. The model also uses the monthly mean GEIA database of the natural volatile organic compound (NVOC) emission which is one of the OC precursors, and the soil dust and sea salt emissions are calculated using internal parameters of the model which are vegetation, wind speed at 10-m height, soil moisture, and snow amount [*Takemura et al.*, 2000]. The DMS emission depends on the surface downward solar flux [*Takemura et al.*, 2000].

[8] The assumed mode radii of the lognormal size distribution depending on the relative humidity used in the radiative calculation are shown in Table 2. The hygroscopic growth of aerosol particles is according to *Tang and Munkelwitz* [1994] for sulfate and *Hobbs et al.* [1997] for carbonaceous particles, which is internal mixture of BC and OC, and second organic carbon from NVOC (SOC). In this model, SOC and 50% BC mass from fossil fuel source are treated as externally mixed particles, and other carbonaceous aerosols are internally mixed particles of BC and OC. The mode radius and standard deviation of externally mixed hydrophobic BC are set at 0.0118μm and 2.0, respectively. The mode radii of soil dust and sea salt aerosols are variable because their mass mixing ratios are predicted dividing into size bins [*Takemura et al.*, 2002a], but their standard deviations are fixed to be 2.50 and 2.51, respectively, in the radiative process. Their fixed mode radius of each dry particle and standard deviation is based on the work of *Martins et al.* [1996] for carbonaceous aerosols and

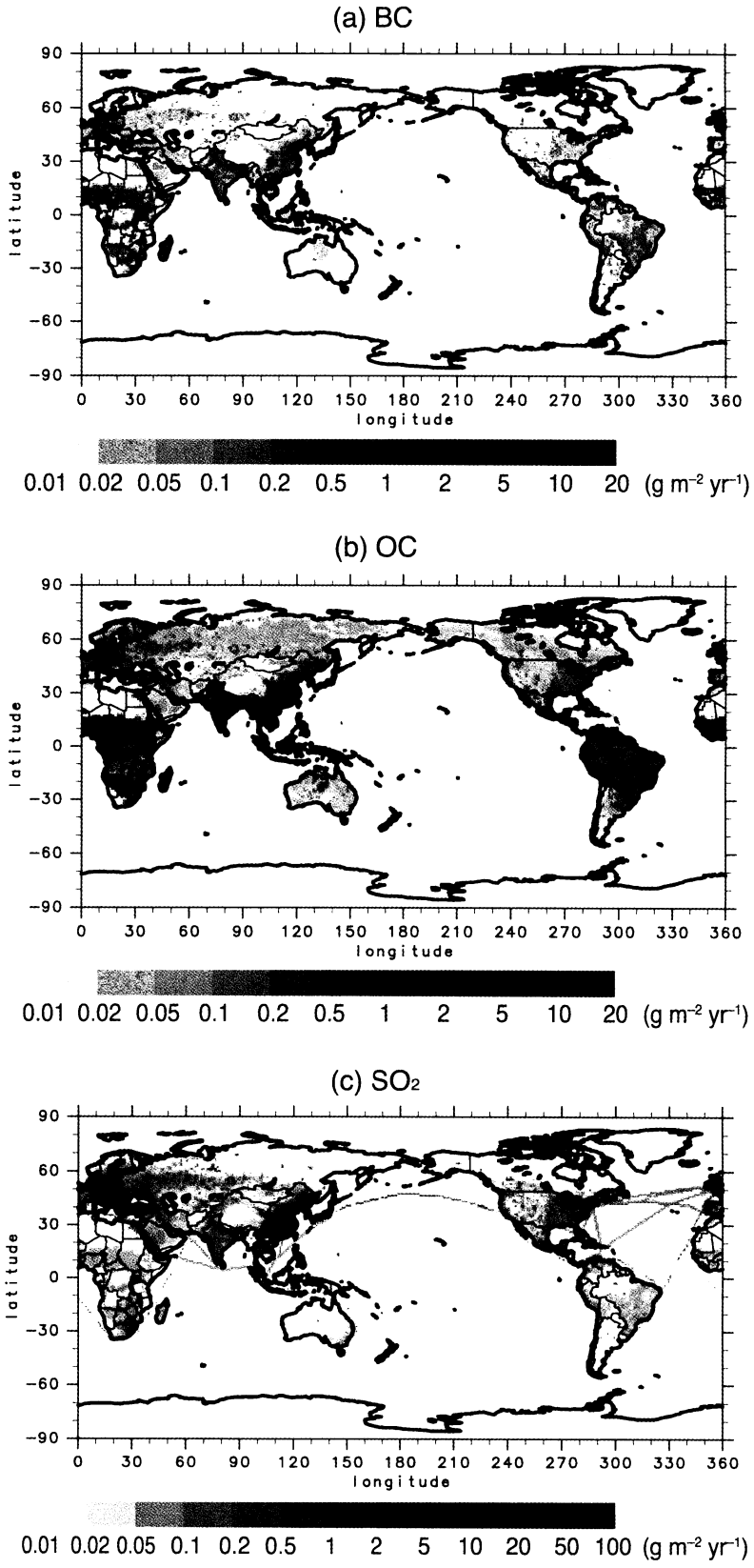

Figure 1. Annual emission fluxes of (a) black carbon (BC) and (b) organic carbon (OC) in g m^{-2} yr^{-1} and (c) SO_2 in gS m^{-2} yr^{-1}.

Table 1. Global and Annual Total Emission Fluxes of BC, OC, and SO_2[a]

	Year	
	1850	2000
BC, Tg yr^{-1}		
BB	0.60	7.48
FF	0.10	5.32
BF	0.40	2.61
AG	0.05	0.57
OC, Tg yr^{-1}		
BB	4.14	51.76
FF	0.33	17.73
BF	2.23	14.74
AG	0.36	3.97
SOC	17.5	17.5
SO_2, Tg S yr^{-1}		
FF	1.27	71.60
BB	0.23	2.88
Volcanic	4.76	4.76

[a]Abbreviations are BB, biomass burning; FF, fossil fuel; BF, biofuel; AG, agricultural waste; SOC, natural secondary OC.

d'Almeida et al. [1991] for other aerosols. The external mixture is assumed for sulfate, soil dust, and sea salt. The radiative calculation is according to the Mie theory using the refractive index of each aerosol component depending on the wavelength. Table 3 shows refractive indices of each aerosol component at 0.55 μm. The refractive indices of water and dry aerosol particles are based on *d'Almeida et al.* [1991] and *World Meteorological Organization* [1983], respectively, except for the imaginary part of soil dust aerosols because their weaker absorption of the solar radiation than *World Meteorological Organization* [1983] has been recently reported [e.g., *Kaufman et al.*, 2001]. The volume-weighted refractive indices are assumed for the internal mixture between aerosol particles and water and between BC and OC.

[9] The present study considers both the first and second indirect effects only for water stratus clouds. While the simple relationship between the total aerosol number concentration and cloud droplet number concentration was used in the previous version of SPRINTARS [*Takemura et al.*, 2003], a parameterization based on the Köhler theory is introduced into this study [*Ghan et al.*, 1997; *Abdul-Razzak et al.*, 1998; *Abdul-Razzak and Ghan*, 2000]. The cloud droplet number concentration N_{ci} originating from an aerosol component i is diagnosed as follows:

$$N_{ci} = N_{ai}\left\{1 + \left(S_{mi}^2 \sum_{j=1}^{J} \frac{F_j}{S_{mj}^2}\right)^{\frac{b(\sigma_{ai})}{3}}\right\}^{-1}, \quad (1)$$

Table 3. Refractive Indices at 0.55 μm of Each Aerosol Component

Component	Index
BC	$1.750-0.440i$
OC	$1.377-3.60 \times 10^{-3}i$
Sulfate	$1.430-1.00 \times 10^{-8}i$
Soil dust	$1.530-2.00 \times 10^{-3}i$
Sea salt	$1.381-4.26 \times 10^{-9}i$

where

$$S_{mi} = \frac{2}{\sqrt{B_i}}\left(\frac{A}{3r_{mi}}\right)^{\frac{3}{2}}, \quad (2)$$

$$F_j = \left\{f_1(\sigma_{aj})\left(\frac{AN_{aj}\beta}{3\alpha\omega}\right)^2 + f_2(\sigma_{aj})\frac{2A^3N_{aj}\beta\sqrt{G}}{27B_jr_{mj}^3(\alpha\omega)^{\frac{3}{2}}}\right\}^3, \quad (3)$$

where j also shows an aerosol component, J is the total number of aerosol components, N_{ai} is the aerosol particle number concentration of component i, ω is the updraft velocity, r_{mi} and σ_{ai} are the mode radius and standard deviation of the aerosol particle size distribution, respectively, A and B_i are the coefficients of the curvature and solute effects, respectively, α and β are functions with the saturated water vapor mixing ratio, temperature, and pressure, G is a function with the water vapor diffusivity, saturated water vapor pressure, and temperature, and f_1, f_2, and b depend on the standard deviation of the aerosol particle size distribution. The minimum numbers of N_a are assumed to be 300 cm^{-3} over land and 30 cm^{-3} over the ocean, which is regarded as the number concentration of the background aerosols [*Hobbs*, 2000]. Chemical properties of each aerosol component in B_i are according to *Ghan et al.* [2001], which depends on the number of dissolved ions per molecule, osmotic coefficient, soluble mass fraction, component density, and molecular weight (Table 4). The mode radii and standard deviations of each aerosol component used in equations from (1) to (3) and in the calculation of aerosol particle number concentrations are the same as Table 2 and descriptions in the previous paragraph. The updraft velocity ω is given as the sum of the grid mean updraft velocity and subgrid updraft velocity because the grid scale of AGCM is too coarse to explicitly represent cloud-scale phenomena [*Lohmann et al.*, 1999]:

$$\omega = \overline{\omega} + c\sqrt{TKE} \quad (4)$$

Table 2. Mode Radii in Microns Depending on the Relative Humidity and Standard Deviation σ_a of Carbonaceous, SOC, and Sulfate Aerosols

	Relative Humidity, %							
Aerosol	0	50	70	80	90	95	98	99
Carbonaceous, μm (σ_a = 1.80)	0.100	0.108	0.110	0.144	0.169	0.196	0.274	0.312
SOC, μm (σ_a = 1.80)	0.0200	0.0216	0.0220	0.0288	0.0338	0.0392	0.0548	0.0624
Sulfate, μm (σ_a = 2.03)	0.0695	0.0850	0.0950	0.103	0.122	0.157	0.195	0.231

Table 4. Hygroscopicity B_i of Each Aerosol Component

Component	B_i
BC	5×10^{-7}
OC	0.14
Sulfate	0.51
Soil dust	0.14
Sea salt	1.16

where *TKE* is the turbulent kinetic energy. N_{ai} and ω at the cloud base are adapted to equations (1) and (3) when N_{ci} is diagnosed. The total number concentration of cloud droplet N_c is derived from summation of equation (1) for each aerosol component [*Abdul-Razzak and Ghan*, 2000]. The cloud droplet effective radius r_{eff}, which is related with the first indirect effect, is then calculated depending on N_c as follows:

$$r_{\text{eff}} = k\left(\frac{3\rho l}{4\pi\rho_w N_c}\right)^{\frac{1}{3}} \tag{5}$$

where ρ is the air density, l is the cloud water mixing ratio, ρ_w is the water density, and k is the empirical constant which is 1.1 in this study [*Martin et al.*, 1994]. The constant k means the fixed shape of the cloud droplet size distribution, while the effect of anthropogenic aerosols on its shape was reported to reduce the aerosol indirect radiative forcing of 0.2 W m^{-2} [*Peng and Lohmann*, 2003]. The precipitation rate P, which is related to the second indirect effect, is parameterized depending on N_c as follows [*Berry*, 1967]:

$$P = -\frac{dl}{dt} = \frac{\alpha\rho l^2}{\beta + \gamma\dfrac{N_c}{\rho l}} \tag{6}$$

where $\alpha = 0.01$, $\beta = 0.12$, and $\gamma = 1 \times 10^{-12}$. Changes in the cloud droplet effective radius and cloud water amount affect the radiation process in the model.

[10] The horizontal resolution of the triangular truncation is set at T42 (approximately 2.8° by 2.8° in latitude and longitude) and the vertical resolution at 20 layers (sigma levels based on the surface pressure at 0.995, 0.980, 0.950, 0.900, 0.830, 0.745, 0.650, 0.549, 0.454, 0.369, 0.295, 0.230, 0.175, 0.124, 0.085, 0.060, 0.045, 0.035, 0.025, and 0.008). In this study SPRINTARS is coupled with the mixed layer ocean model under the prescribed surface heat flux that was previously calculated using the given monthly mean sea surface temperature (SST) and sea ice by SPRINTARS. Three equilibrium experiments are carried out for different scenarios of aerosols and greenhouse gases; present-day aerosol emissions and present-day greenhouse gas concentrations (E1), preindustrial aerosol emissions and present-day greenhouse gas concentrations (E2), and preindustrial aerosol emissions and preindustrial greenhouse gas concentrations (E3). Each experiment is integrated for 50 years and analyzed for the last 30 years. Only the radiative forcing is estimated with the prescribed tropospheric temperature, SST, and sea ice experiment according to the general method of calculating the radiative forcing with AGCMs [*Hansen et al.*, 2002]. The globally homogeneous greenhouse gas concentrations are shown in Table 5.

3. Simulated Aerosol and Cloud Parameters

3.1. Aerosol Particle and Cloud Droplet Distributions

[11] Figure 2 shows the annual mean distributions of the optical thickness at 0.55 μm for each aerosol component in the present-day simulation. Carbonaceous aerosols concentrate over populous regions in the midlatitudes of the Northern Hemisphere because of consumption of fossil and bio fuels and agricultural activities. They also exist over biomass burning regions in central and southern Africa and South America. The optical thickness of sulfate aerosols is large over urban areas in the midlatitude of the Northern Hemisphere, and they are also broadly distributed over the ocean because of the chemical reaction of DMS. A large amount of soil dust aerosols are emitted from the Saharan region and then transported to the tropical Atlantic. They also concentrate over the Arabian and Asian regions. The optical thickness of sea salt aerosols over the ocean is more homogeneous than that of other aerosols. The simulated aerosol optical properties of not only optical thickness but also Ångström exponent that is an index of particle size and single scattering albedo are in reasonable agreement with the ground-based observations of the Aerosol Robotic Network (AERONET) [*Holben et al.*, 2001] and satellite retrievals of AVHRR [*Higurashi et al.*, 2000], which has been described in detail by *Takemura et al.* [2002a]. The reproduction of aerosol distributions by SPRINTARS was also indicated to be realistic as shown in the intercomparison among several global aerosol transport models and satellite retrievals [*Kinne et al.*, 2003].

[12] Before discussion on the effect of anthropogenic aerosols on climate in section 4, differences of global distributions of mass concentrations for BC, OC, and sulfate between preindustrial and present-day simulations are shown in Figure 3. BC is a minor aerosol composition at the preindustrial era, a few tenths of micrograms per cubic meter even in urban and biomass burning areas. An increasing rate of OC from preindustrial to the present day is slightly smaller than that of BC because main sources of carbonaceous aerosols at the preindustrial era are biofuel, traditional

Table 5. Volume Concentrations of Greenhouse Gases

	Year	
	1850	2000
CO_2, ppmv	285.43	336.77
N_2O, ppmv	0.28	0.32
CH_4, ppmv	0.86	1.79
CFC, ppmv ($\times 10^{-6}$)		
CFC11, ppmv	0.0	266.7
CFC12, ppmv	0.0	535.0
CFC113, ppmv	0.0	85.2
CFC114, ppmv	0.0	15.8
CFC115, ppmv	0.0	8.6
HCFC22, ppmv	0.0	144.9
HCFC123, ppmv	0.0	0.3
HCFC125, ppmv	0.0	2.2
HCFC134a, ppmv	0.0	35.1
HCFC141b, ppmv	0.0	13.2
HCFC142b, ppmv	0.0	14.9
CCl_4, ppmv	1.7	91.7
CH_3CCl_3, ppmv	0.0	43.5

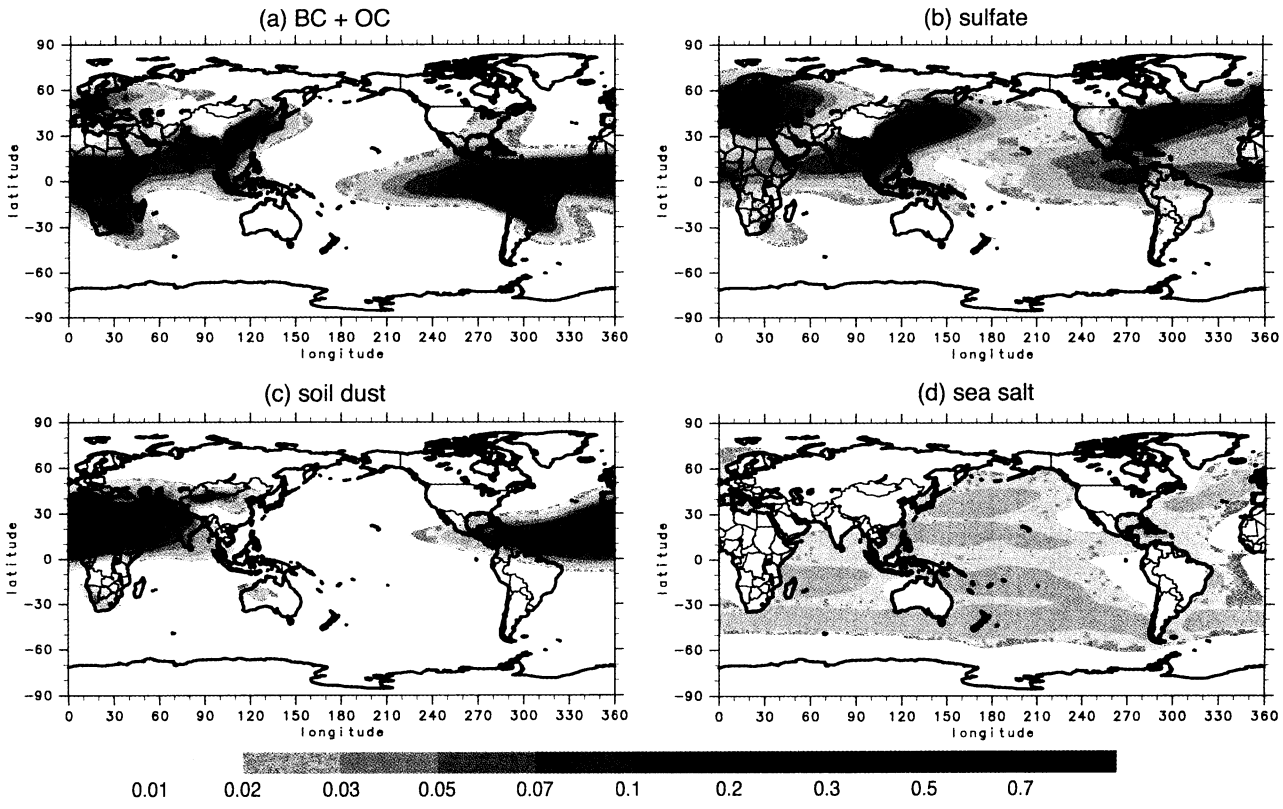

Figure 2. Annual mean distributions of the simulated optical thickness for (a) BC plus OC, (b) sulfate, (c) soil dust, and (d) sea salt aerosols at 0.55 μm.

slash-and-burn farming, natural biomass burning, and biogenic terpene, which are effective OC sources. Sulfate aerosols at the preindustrial day are more prominent over the ocean than over land because of natural DMS emission from oceanic phytoplankton and outflow of volcanic SO_2.

[13] Number concentrations of aerosol particles N_a and cloud droplet N_c are important parameters in case of discussion on the cloud microphysics, which are shown in Figure 4. N_a is dominated by nucleation and accumulation mode particles of carbonaceous and sulfate aerosols, so that N_a of soil dust aerosols is small though their optical thickness is large (Figure 2c). The spatial distribution of N_c is similar to that of N_a, while the contrast of N_c between land and ocean is weaker than that of N_a. Aircraft measurements also obtained that an increasing rate of N_c is getting small with an increase in N_a [*Martin et al.*, 1994]. The relationship between N_a and N_c is dispersed using equation (1) because of differences in the updraft velocity, aerosol particle size distribution, chemical property, and saturated condition of water vapor among the grids (Figure 5).

3.2. Cloud Droplet Effective Radius

[14] It is important to quantitatively simulate the cloud droplet radius for estimating the aerosol first indirect effect. Figure 6 illustrates the annual mean distributions of the cloud droplet effective radius at cloud top above 273 K simulated by SPRINTARS and retrieved from AVHRR [*Nakajima and Nakajima*, 1995]. The cloud droplet cannot be analyzed by AVHRR at high latitudes because of the large solar zenith angles. The simulated small radius from 6 to 12 μm over continents is consistent with the AVHRR retrieval. It is especially small in the industrialized areas of Europe, east Asia, and North America. It is, on the other hand, large above 14 μm mostly over the ocean, particularly in the Southern Hemisphere where it is only slightly affected by anthropogenic pollutants, though SPRINTARS overestimates it in the tropical western Pacific because of an excess of cloud water in the middle troposphere. The cloud droplet, however, is somewhat small even over the ocean off the industrialized areas because of outflows of anthropogenic aerosols and of the subtropical eastern Pacific and Atlantic because of cloud water concentrated in the lower troposphere, which is in good agreement between SPRINTARS and AVHRR. N_c was determined only by N_a or the aerosol mass concentration for the simulation of the aerosol indirect effect in past AGCM studies [e.g., *Rotstayn and Lohmann*, 2002; *Takemura et al.*, 2003]. Using the parameterization based on the Köhler theory in this study, the simulated land-ocean contrast of the cloud droplet effective radius becomes closer quantitatively to the satellite observation than that by the past simple parameterization, and the large one between 30° and 60°S can be also simulated well.

[15] The correlation of the cloud droplet effective radius between the simulation and satellite observation is high on a global scale except for a difference in the larger radius of about 20 μm in the tropical western Pacific by SPRINTARS than by AVHRR mentioned above and another difference below 10 μm by AVHRR and 10 to 15 μm by SPRINTARS around the desert regions (Figure 7). In the case when the cloud water is low, such as in the desert regions, the

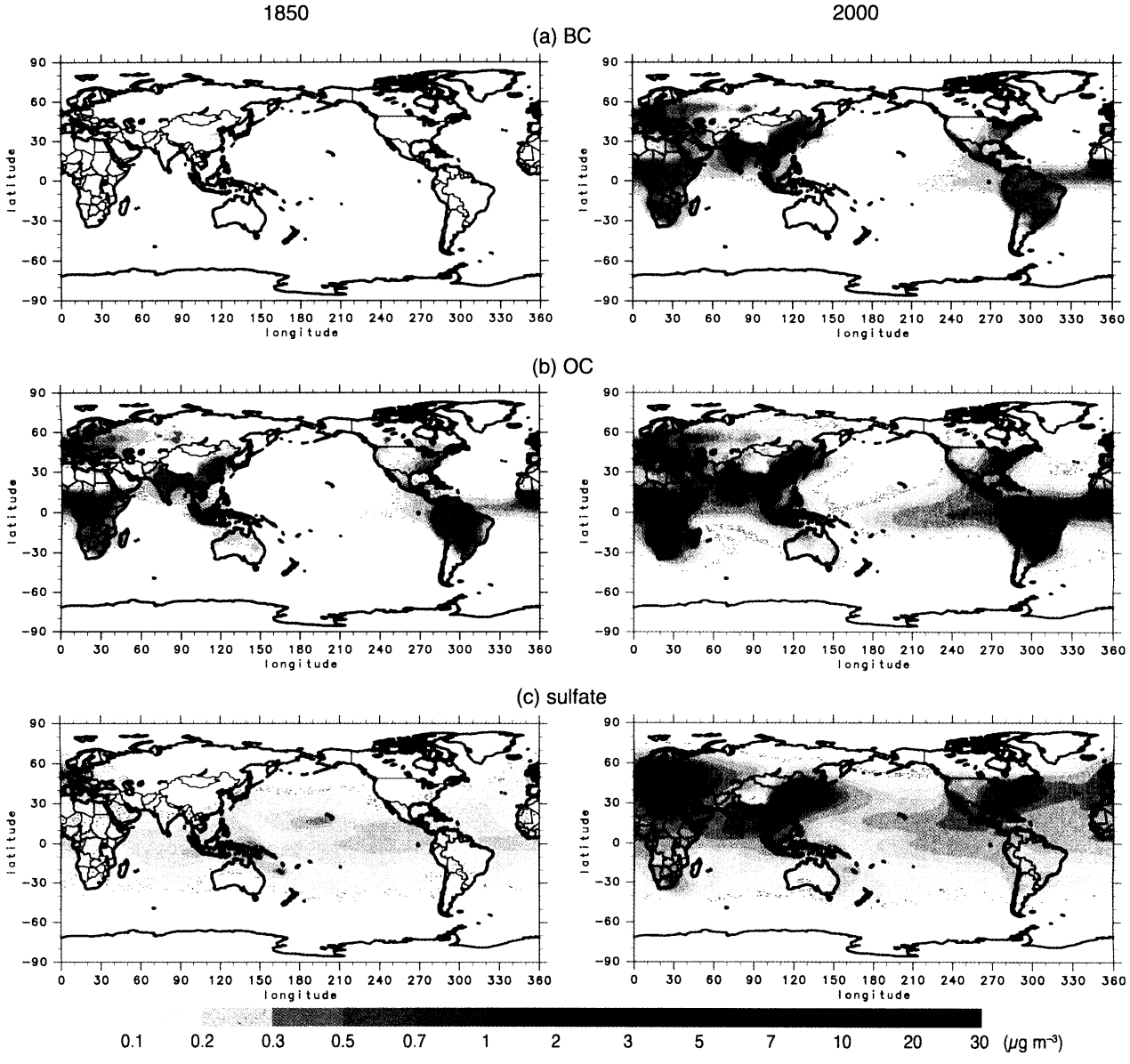

Figure 3. Annual mean distributions of the simulated surface mass concentrations of (a) BC, (b) OC, and (c) sulfate in (left) 1850 and (right) 2000.

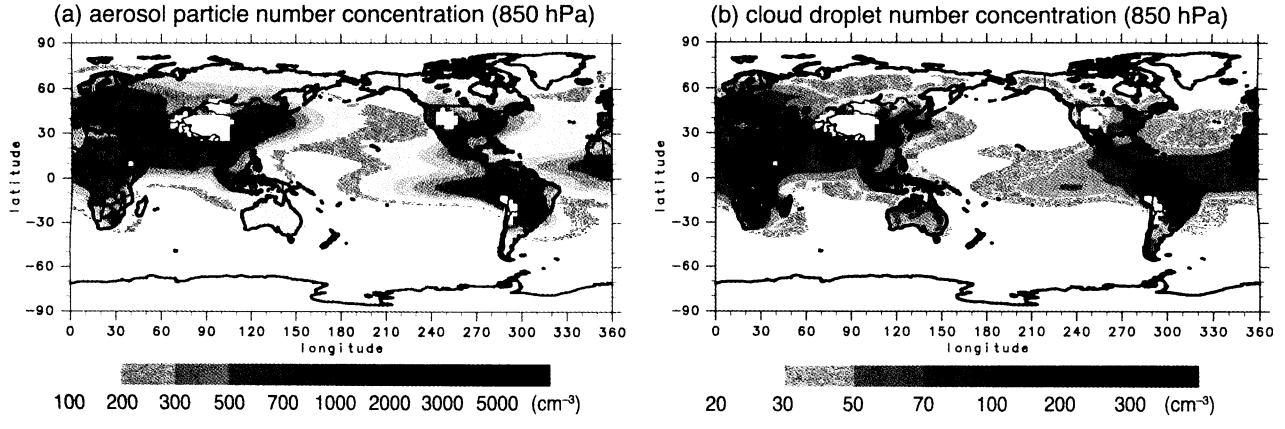

Figure 4. Annual mean distributions of the simulated number concentrations of (a) aerosol particles and (b) cloud droplet at 850 hPa.

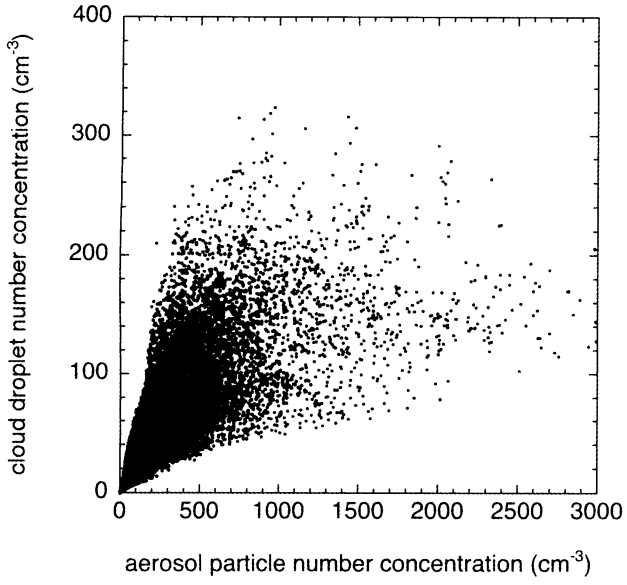

Figure 5. Relationship between aerosol particle and cloud droplet number concentrations at the sigma level between 0.95 and 0.55 in the simulation.

precision of the satellite retrieval for cloud water may get poor unless the surface albedo and temperature are appropriately assumed [*Nakajima and Nakajima*, 1995].

[16] Figure 8 shows the frequency distributions of the cloud droplet effective radius for the present-day and preindustrial simulations over land and the ocean. The mode radius over land is about 11 μm in the preindustrial era, and then the distribution broadens to small radii of about 8 μm because of an increase in anthropogenic aerosols. The small droplets from 9 to 12 μm over the ocean also increase in the present-day simulation though the mode radius does not change much.

3.3. Cloud Water and Precipitation

[17] Before discussion of the aerosol second indirect effect, the simulated cloud water and precipitation are confirmed to be appropriate in comparison with observations when equations (1) to (6) are applied. The nucleation process of the cloud water microphysics is only considered in equation (1); that is, the model does not include processes of autoconversion, accretion, evaporation, freezing, and melting of ice, so that the cloud droplet number concentration N_c may be overestimated [*Ghan et al.*, 1997]. Therefore, in this study, the sensitivity of the precipitation rate P

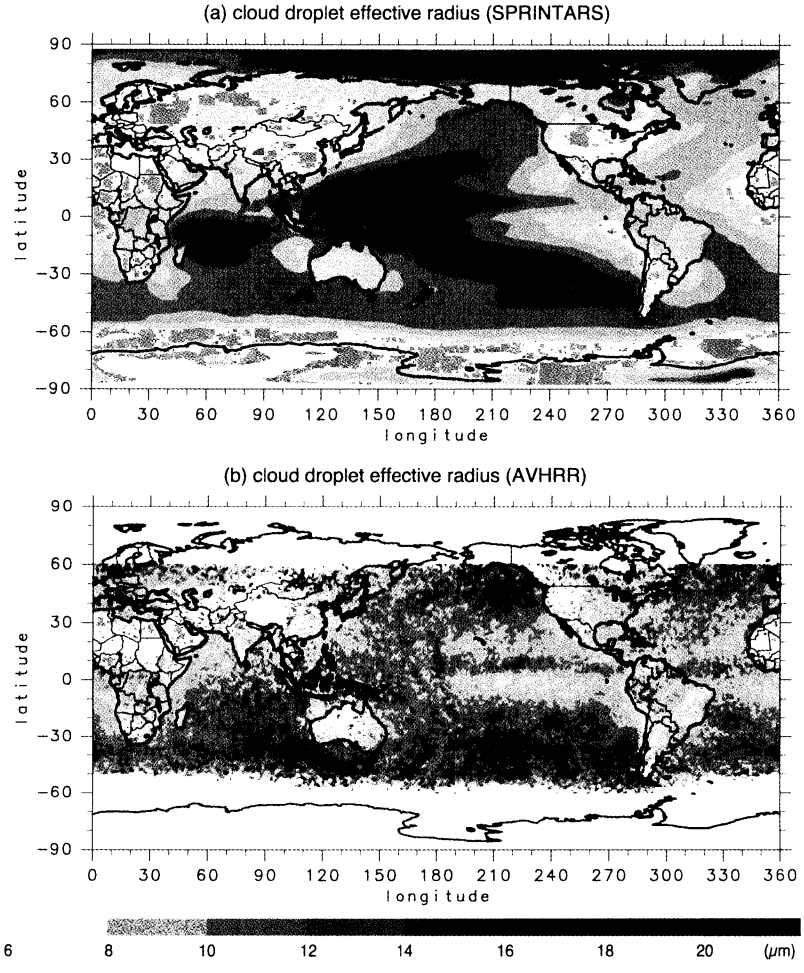

Figure 6. Annual mean distributions of the cloud droplet effective radius at the cloud top above the temperature of 273 K by the (a) Spectral Radiation-Transport Model for Aerosol Species (SPRINTARS) and (b) advanced very high resolution radiometer (AVHRR) retrieval.

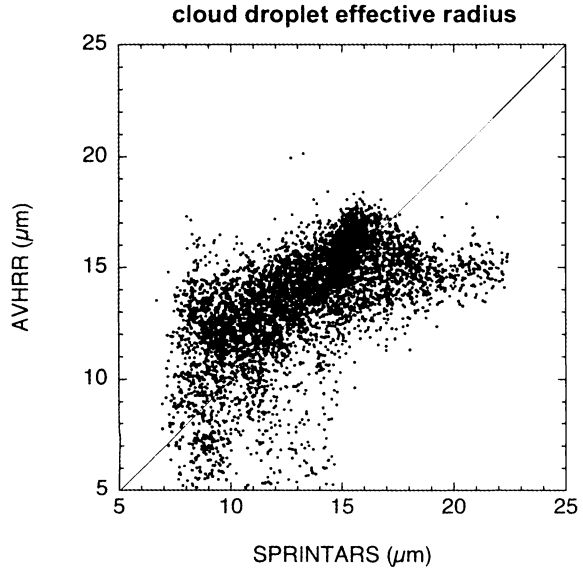

Figure 7. Comparison of the cloud droplet effective radius at the cloud top above the temperature of 273 K between the SPRINTARS and AVHRR retrieval.

to N_c is decreased with smaller γ in equation (6) than the other study [*Lohmann et al.*, 1999]; α in equation (6) is also adjusted to balance the net incoming shortwave radiation with the net outgoing longwave radiation. Figure 9 illustrates the annual mean liquid water path and precipitation simulated by the model, and the simulated cloud radiative forcing and precipitation are compared with data from the Earth Radiation Budget Experiment (ERBE) [*Harrison et al.*, 1990] and Global Precipitation Climatology Project (GPCP) [*Adler et al.*, 2003] in Figures 10 and 11, respectively. The model calculates the seasonal and latitudinal cloud and rain generally well, though there are some differences both in cloud and precipitation between the simulation and observations in high latitudes of the Southern Hemisphere which is less affected by anthropogenic aerosols than the other regions. On the basis of these comparisons of cloud and precipitation in the previous and present sections, changes in these parameters by anthropogenic aerosols are discussed in section 4.

3.4. Direct and Indirect Radiative Forcing

[18] The aerosol radiative forcing is estimated by the simulation with the prescribed tropospheric temperature, SST, and sea ice as mentioned in section 2. Figure 12 shows the annual mean radiative forcing by the direct and indirect effects of anthropogenic aerosols at the tropopause. The direct radiative forcing in this study is defined as a comparison between preindustrial and present simulations on a difference in net fluxes with and without aerosols. It exceeds -1 W m^{-2} in east and south Asia, Europe, and North America because of industrial and domestic OC and sulfate aerosols though the anthropogenic BC produces a positive forcing. The negative forcing is also large over most of southern Africa and South America mainly because of biomass burning aerosols which is a mixture of BC, OC, and sulfate. On the other hand, the outflow of carbonaceous aerosols from biomass burning and industrialized regions makes the direct radiative forcing positive over the Saharan and Arabian deserts with their high surface albedo. Biomass burning aerosols also cause the positive forcing off central and southern Africa and South America because the multiple scattering of the solar radiation by the lower cloud layer than the aerosol layer enhances its absorption by biomass burning aerosols [*Haywood and Ramaswamy*, 1998; *Takemura et al.*, 2002a]. If it is under clear-sky conditions or the cloud layer is relatively higher than the aerosol layer, the direct radiative forcing by biomass burning aerosols is negative. The global mean anthropogenic forcing at the tropopause by the aerosol direct effect is calculated to be -0.06 W m^{-2} and -0.77 W m^{-2} under all-sky and clear-sky conditions, respectively. Table 6 indicates the mean direct radiative forcing by anthropogenic aerosols at the tropopause and the surface. The BC positive forcing is comparable to the negative forcing of OC plus sulfate under all-sky conditions at the tropopause. The simulated sulfate forcing of -0.21 W m^{-2} by the present model is the minimum value of the estimation of *IPCC* [2001]. Under clear-sky conditions, the positive forcing of BC reduces and the negative forcing of OC and sulfate increases because absorbing the multiscattered radiation by BC particles caused by cloud layers is absent and the stronger direct solar radiation reaches the OC and sulfate particles. At the surface, on the other hand, BC has a stronger negative forcing than the OC and sulfate. The absolute values of the mean direct radiative forcing over land are about twice as high as over the ocean for each aerosol component mainly because of the differences in aerosol loadings.

[19] The indirect radiative forcing by anthropogenic aerosols in this study is calculated as a comparison between two experiments, preindustrial and present runs, on a difference in the cloud radiative forcing. The indirect radiative forcing is generally negative except in the polar region and areas less affected by anthropogenic aerosols. The large negative forcing is seen over the northwestern Pacific, Southeast Asia, Eurasia, North America, South America, and southern Africa. The global mean anthropogenic forcing by the

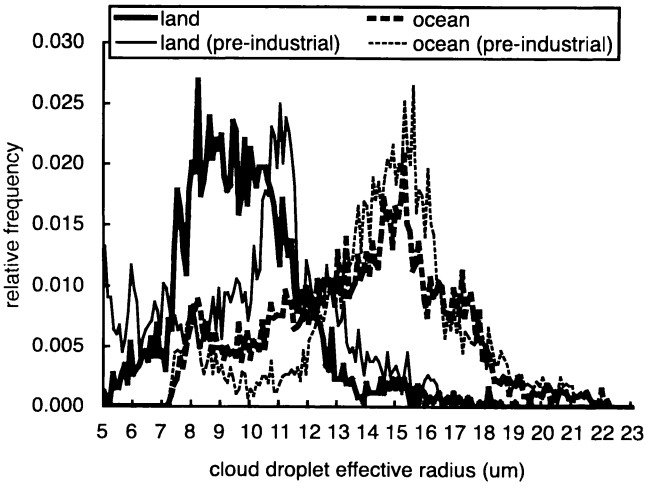

Figure 8. Frequency distributions of the cloud droplet effective radius over land (solid lines) and ocean (dashed lines) for the present (thick lines) and preindustrial (thin lines) simulations.

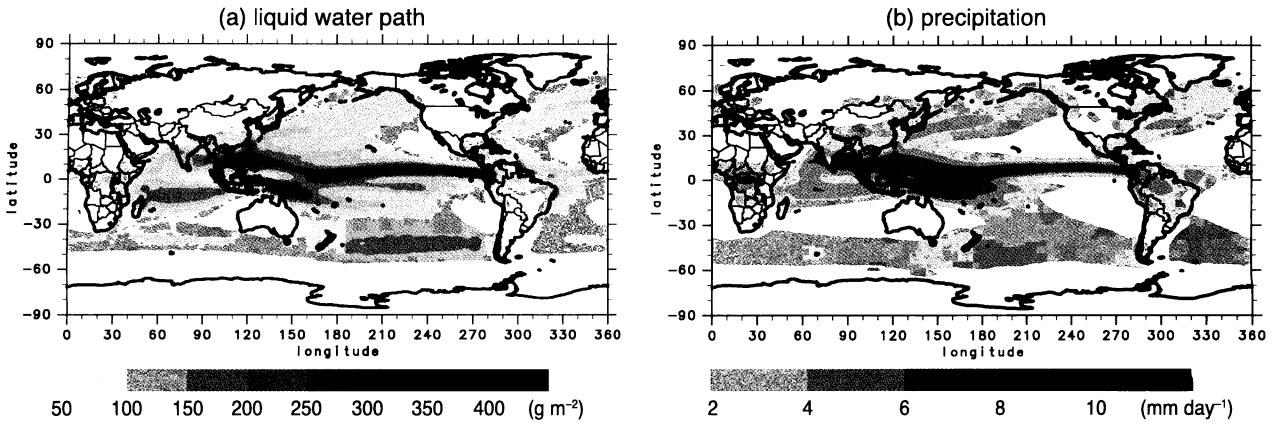

Figure 9. Annual mean distributions of the simulated (a) liquid water path and (b) precipitation.

aerosol first plus second indirect effects is calculated to be -0.94 W m^{-2}. If the other formula of *Sundqvist* [1978] is used for calculating the precipitation rate instead of equation (6), which does not depend on the aerosol number concentration, only the first indirect effect can be estimated to be -0.52 W m^{-2}. Most past studies cited by the IPCC TAR [*IPCC*, 2001] estimated the indirect radiative forcing over -1 W m^{-2} for the global mean from the preindustrial to the present day. If it is over -1 W m^{-2}, however, an unrealistic temperature decrease by the aerosol effects may be simulated as mentioned in the next section. *Lohmann and Lesins* [2002] constrained the simulated aerosol indirect effect by a global climate model using a satellite cloud retrieval, so that its radiative forcing was reduced from -1.4 to -0.85 W m^{-2}.

4. Effects of Anthropogenic Aerosols on Climate

[20] Figure 13 illustrates the changes in the cloud droplet effective radius at cloud top above 273K, liquid water path, and precipitation for the period from preindustrial to the present day by comparing the simulations between E1 and

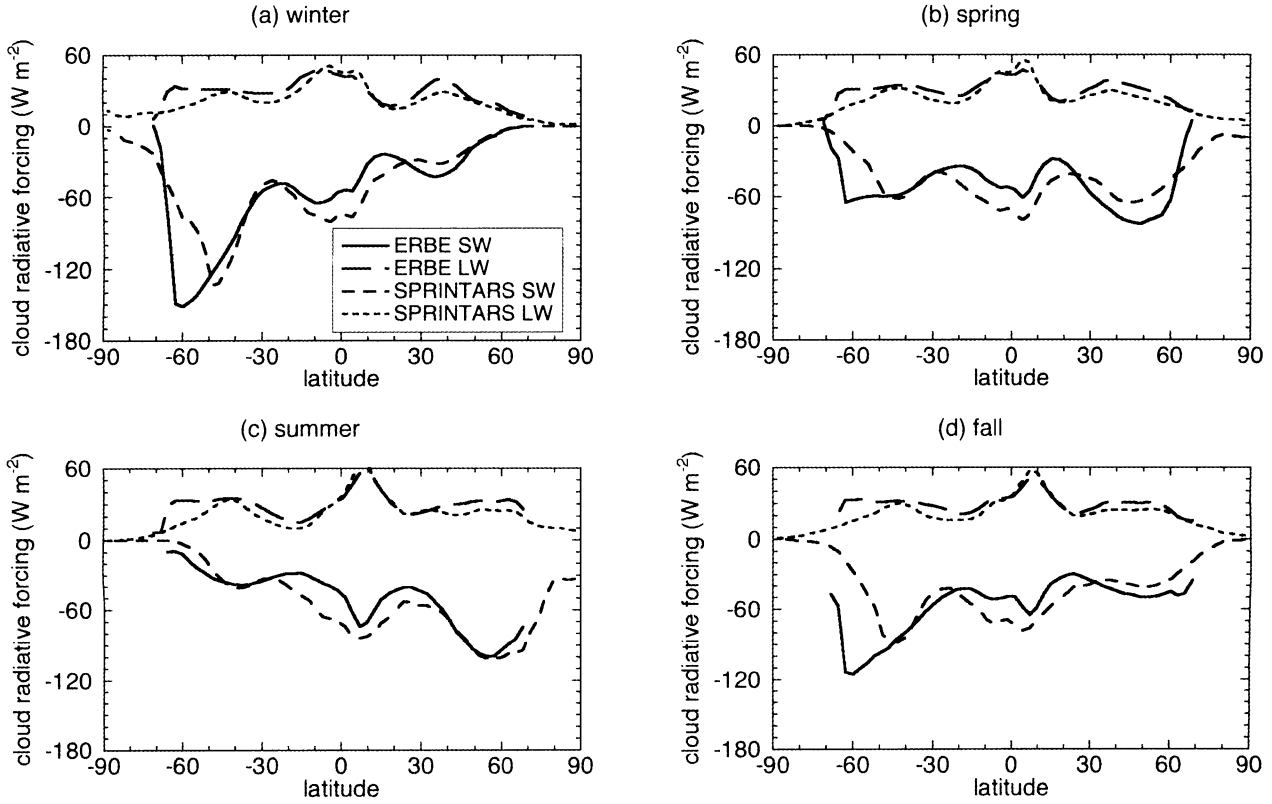

Figure 10. Zonal mean distributions of the seasonal mean cloud radiative forcing of SPRINTARS and Earth Radiation Budget Experiment (ERBE) for both the shortwave (SW) and longwave (LW) radiation in the Northern Hemisphere (a) winter, (b) spring, (c) summer, and (d) fall.

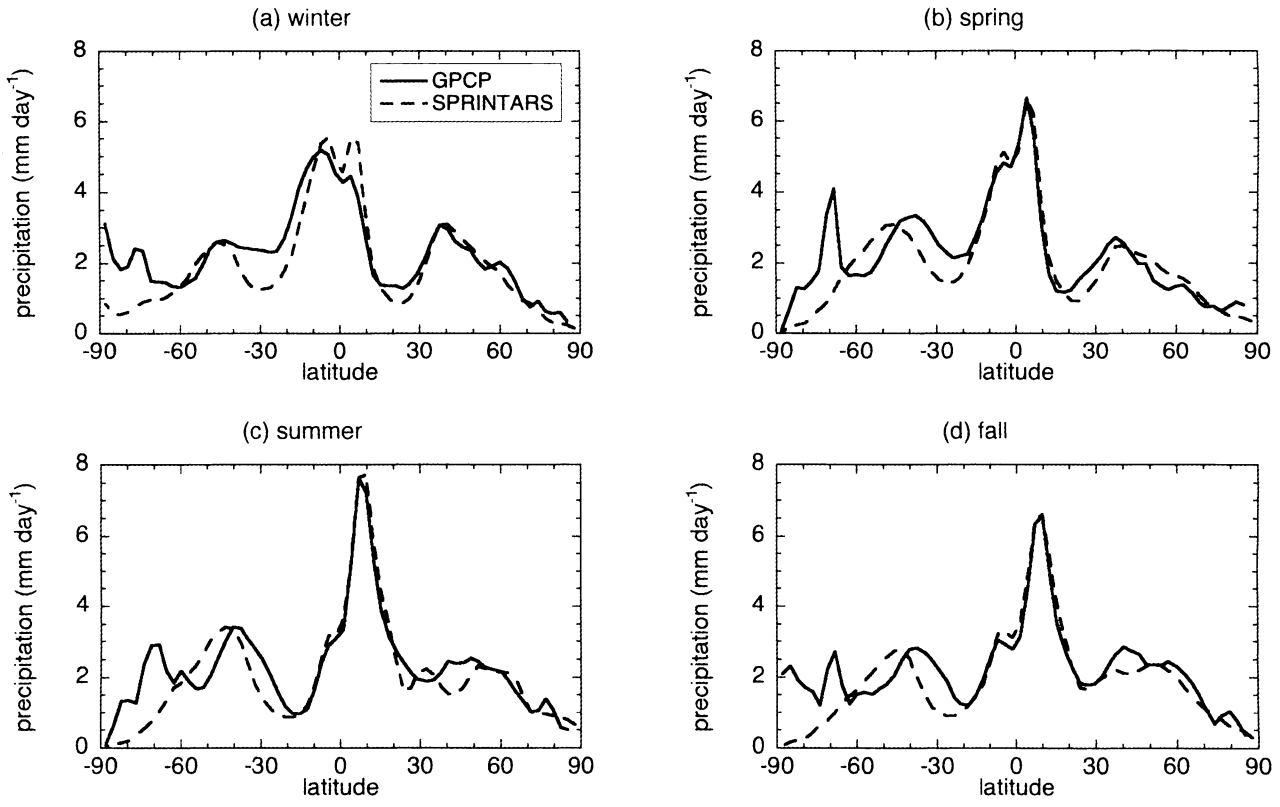

Figure 11. Zonal mean distributions of the seasonal mean precipitation of SPRINTARS and Global Precipitation Climatology Project (GPCP) in Northern Hemisphere (a) winter, (b) spring, (c) summer, and (d) fall.

E2. The blue contours in Figure 13 indicate the general direction of the aerosol indirect effect. Reliance on the estimation of changes in the cloud and precipitation parameters is low in the high latitudes because there is little cloud water. A comparison between E1 and E2 is not in strict correspondence with Figure 12 because the indirect radiative forcing is estimated with prescribed atmospheric temperature, SST, and sea ice. The cloud droplet effective radius, which is related to the first aerosol indirect effect, decreases almost all over the globe. Large changes from 2 to 5 μm are simulated in east and south Asia, Europe, and North America because of their industrial and domestic activities and in central and southern Africa and South America because of the expansion of anthropogenic biomass burning. The global mean change in the cloud droplet effective radius is calculated to be −1.1 μm, comparable between land and the ocean. The increase in cloud droplet radius over the remote ocean of the Southern Hemisphere and the pole regions, where a change in the aerosol concentration is less than that in other regions, is diagnosed by an increase in cloud water at the altitude of 273 K mainly because the altitude is descending and getting close to the cloud base because of the aerosol cooling effects. An increase in cloud water results in an increase in precipitation over a large part of the globe, and vice versa. Especially, there is a strong constraint in tropical regions though the cloud microphysical treatment is not included in the convective scheme of the model [*Rotstayn and Lohmann*, 2002]. The change in the horizontal water vapor flux from the preindustrial to the present day at the lower troposphere is shown in Figure 14. It clearly indicates that an increase (decrease) in liquid water in the southern (northern) tropics is due to convergence (divergence) of water vapor at the lower troposphere. Therefore it is suggested that changes in liquid water and precipitation in the tropics is a feedback effect due to tropospheric cooling by the aerosol effects. The difference in the horizontal water vapor flux is much smaller at the middle troposphere than the lower troposphere (not shown). It is also suggested that a change in water vapor around cloud base is essential for this feedback mechanism. In east and Southeast Asia and the Atlantic in the tropics and midlatitude of the Northern Hemisphere, on the other hand, an increase in the cloud water and a decrease in precipitation simultaneously occur. There is not large-scale convergence of water vapor in these regions as shown in Figure 14. This suggests that the effect of the aerosol second indirect effect on the cloud microphysical process is stronger than the effect of the dynamic hydrological cycle in the regions where a large amount of anthropogenic aerosols and cloud water exist.

[21] Figure 15 shows a change in the surface air temperature from the preindustrial to the present day by comparing experiments E1 and E2. The surface air temperature change over −2 K occurs in east Asia, Europe, and the high latitudes of the Northern Hemisphere, and it also decreases almost all over the globe. This suggests that the decrease in the surface air temperature is mainly caused by the aerosol direct and first indirect effects because the areas where its

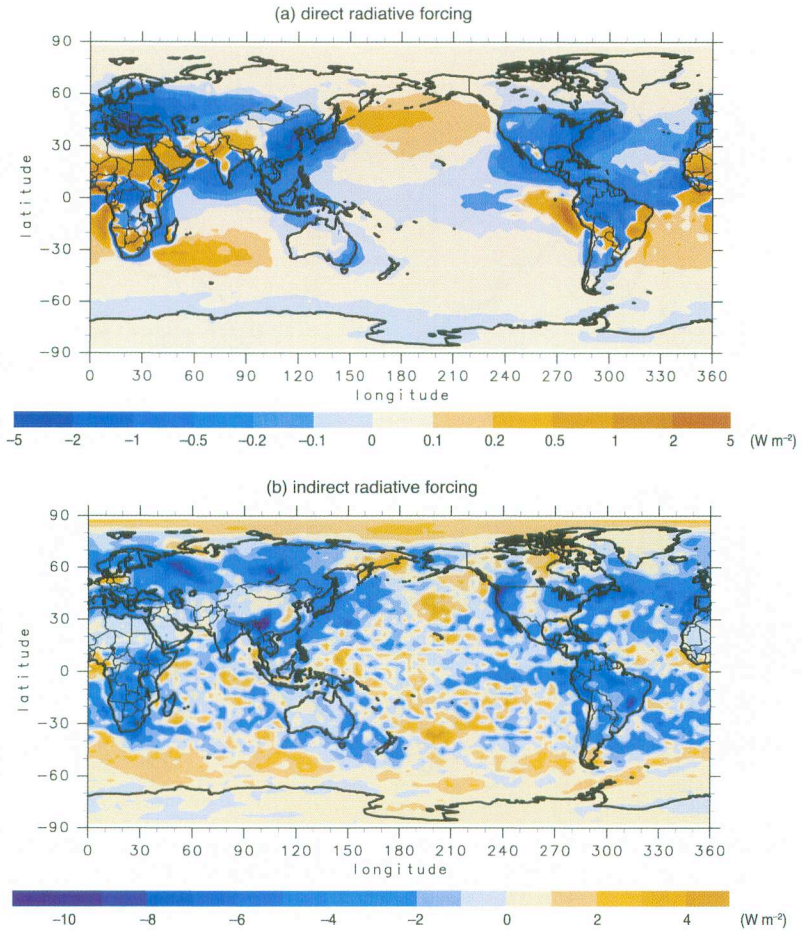

Figure 12. Simulated aerosol (a) direct and (b) indirect radiative forcings from preindustrial to the present day.

change is large are in general agreement with those where the negative direct radiative forcing (Figure 12a) and the decrease in the cloud droplet radius (Figure 13a) are large. The global mean surface air temperature change by the aerosol effects is calculated to be −1.0 K, while it is estimated to be +2.3 K because of the greenhouse gases as the difference between experiments E2 and E3. Therefore the simulated cooling effect by aerosol particles reduces about 40% of the global warming by the greenhouse gases from the preindustrial to the present day, which is consistent with *IPCC* [1996], though the temperature change is quantitatively larger in the simulation than the real past climate not because of the transient but equilibrium experiments.

5. Conclusions

[22] A global aerosol transport-radiation model, SPRINTARS, coupled to a general circulation model simulated climate response to the direct and indirect effects of anthropogenic aerosols. The diagnosing scheme based on the Köhler equation calculated the cloud droplet effective radius, cloud water, and precipitation, which are in reasonable agreement with satellite observations. Table 7 summarizes the radiative forcing and change in the cloud parameters, precipitation, and surface air temperature by anthropogenic aerosols. This study indicated that the global mean direct radiative forcing is nearly −0.1 W m^{-2}, resulting from the balance between cooling by OC and sulfate and warming by BC. The indirect radiative forcing was calculated to be −0.9 W m^{-2}, which is consistent with recent studies using satellite retrievals on aerosol and cloud parameters [*Nakajima et al.*, 2001; *Lohmann and Lesins*, 2002]. The simulation indicated that the changing ratios of all the cloud and precipitation parameters are larger over land than over the

Table 6. Annual Mean Direct Radiative Forcing From Preindustrial to Present Days for All-Sky and Clear-Sky Conditions at the Tropopause and the Surface

	All-Sky Conditions			Clear-Sky Conditions		
	Land	Ocean	Global	Land	Ocean	Global
			Tropopause			
BC, W m^{-2}	+0.76	+0.30	+0.42	+0.67	+0.10	+0.26
OC, W m^{-2}	−0.49	−0.19	−0.27	−0.84	−0.39	−0.51
Sulfate, W m^{-2}	−0.36	−0.15	−0.21	−0.90	−0.37	−0.52
Total, W m^{-2}	−0.09	−0.04	−0.06	−1.07	−0.66	−0.77
			Surface			
BC, W m^{-2}	−1.41	−0.51	−0.76	−1.64	−0.68	−0.94
OC, W m^{-2}	−0.65	−0.24	−0.36	−0.97	−0.42	−0.57
Sulfate, W m^{-2}	−0.27	−0.12	−0.16	−0.69	−0.31	−0.41
Total, W m^{-2}	−2.33	−0.87	−1.28	−3.30	−1.41	−1.92

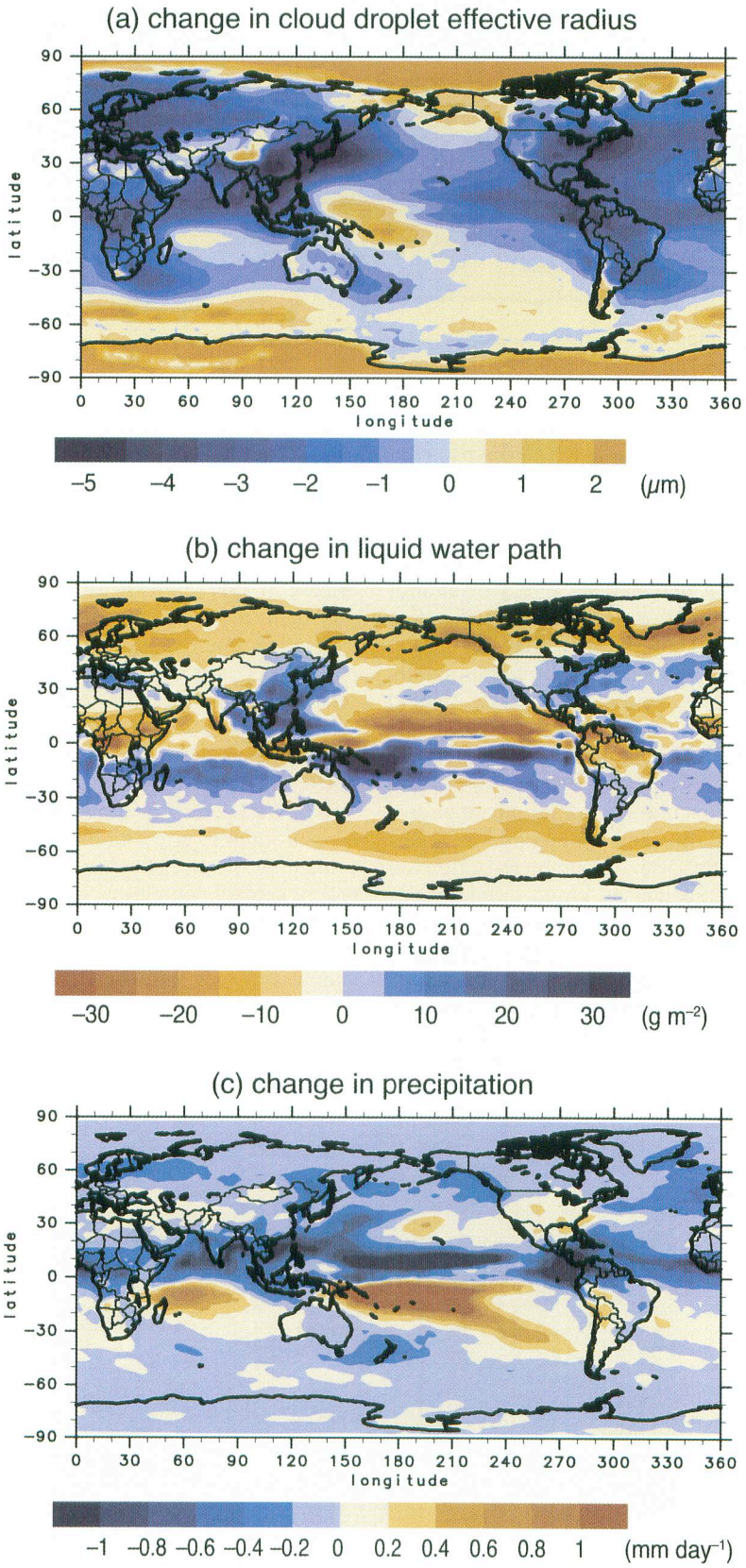

Figure 13. Change in the simulated (a) cloud droplet effective radius at the cloud top above the temperature of 273 K, (b) liquid water path, and (c) precipitation from preindustrial to the present day.

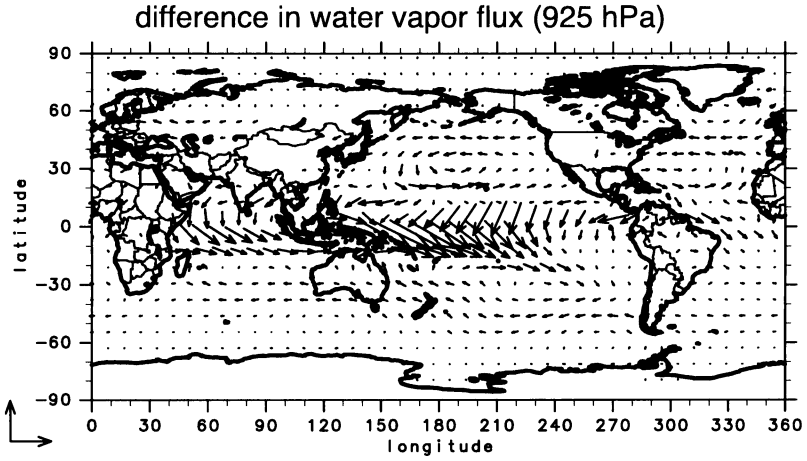

Figure 14. Annual mean distribution of a difference in the horizontal water vapor flux between the preindustrial and the present day at 925 hPa. The unit vector indicated at the bottom left-hand corner is 0.03 kg m kg^{-1} s^{-1}.

ocean because of the direct and indirect effect of anthropogenic aerosols. The cloud droplet effective radius reduces about 10% because of the first indirect effect, while changes in the liquid water and precipitation mainly depend on the change in the hydrological cycle due to cooling by the aerosol direct and first indirect effects. The change in the surface air temperature is also large over land.

[23] The present model includes a lot of assumptions: size distributions, refractive indices, and emission fluxes for each aerosol component, use of parameterization on nucleation process for diagnosing the cloud droplet number concentration in equation (1), parameters in equations from (1) to (6), and so on. *Zhang et al.* [2002] and *Peng and Lohmann* [2003], for example, discussed the uncertainty of the aerosol indirect effect due to assumed aerosol size distribution. It is, however, difficult to quantitatively estimate the uncertainty of the aerosol effects in this study because assumptions are used a lot and then complex. To make the confidence level of the estimation high, many comparisons of aerosol and cloud parameters with various observations have been carried out, including not only aerosol burden but also aerosol Ångström exponent (size index) and single scattering albedo in past studies [*Takemura et al.*, 2002a, 2002b, 2003] and this study.

[24] We have to continue these modeling studies on the aerosol indirect effect in order to reduce the uncertainty of estimating the climate change. One factor to consider is the role of aerosol particles as ice nuclei. *Lohmann and Kärcher* [2002] introduced the homogeneous ice nucleation process by hygroscopic aerosols into a GCM and indicated that sulfate aerosols from aviation are unlikely to change the properties of cirrus clouds. The heterogeneous freezing process including other aerosol species, such as BC, should be considered in the GCM studies in the future. The other

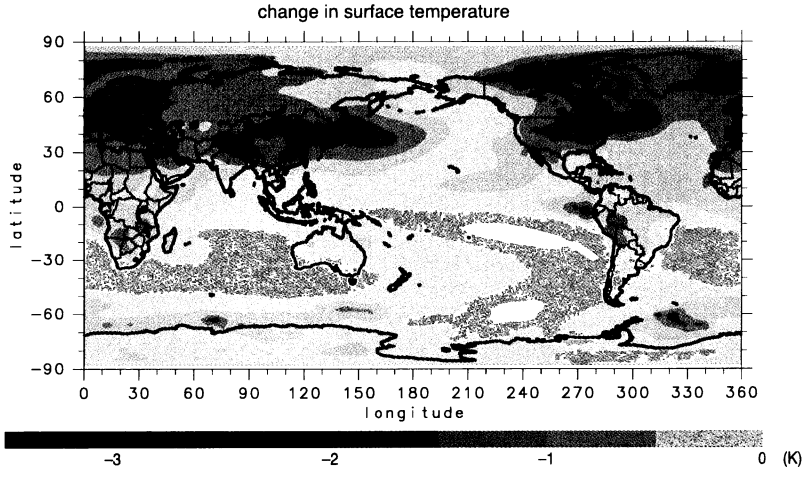

Figure 15. Change in the simulated surface air temperature by anthropogenic aerosols from the preindustrial to the present day.

Table 7. Annual Mean Changes in Radiative Forcings at the Top of the Atmosphere and Meteorological Parameters Related to the Aerosol Effects From Preindustrial to Present Day[a]

	Land	Ocean	Global
Direct radiative forcing, W m^{-2}	−0.08	−0.02	−0.04
Indirect radiative forcing, W m^{-2}	−1.72 (−1.14)	−0.65 (−0.28)	−0.94 (−0.52)
Cloud effective radius, μm	−1.2 (−12%)	−1.1 (−8%)	−1.1 (−8%)
Liquid water path, g m^{-2}	−4.2 (−6%)	−1.8 (−1%)	−2.4 (−2%)
Precipitation, mm d^{-1}	−0.10 (−6%)	−0.11 (−4%)	−0.11 (−4%)
Temperature at 2 m, K	−1.5	−0.9	−1.0

[a]Numbers in parentheses indicate the first indirect radiative forcing in the section of indirect radiative forcing or changing ratios in other sections.

factor is to simulate the continuative growth process both of aerosol particles and cloud droplets with the bin models. There are some cloud microphysical models [e.g., *Khain et al.*, 2000], but it is important to explicitly treat the nucleation process with aerosol particles by the bin method.

[25] **Acknowledgments.** We thank the contributors to the development of the CCSR/NIES/FRCGC GCM, J. Kurokawa of Fujitsu FIP Corporation for providing the historical emission data related to aerosols, S. J. Ghan of Pacific Northwest National Laboratory for allowing us to use the aerosol-cloud parameterization, and anonymous reviewers. This study is partly supported by the APEX project of the Core Research for Evolutional Science and Technology of the Japan Science and Technology Agency. The simulation in this study was done on NEC SX-6 of the National Institute for Environmental Studies.

References

Abdul-Razzak, H., and S. J. Ghan (2000), A parameterization of aerosol activation: 2. Multiple aerosol type, *J. Geophys. Res.*, *105*, 6837–6844.

Abdul-Razzak, H., S. J. Ghan, and C. Rivera-Carpio (1998), A parameterization of aerosol activation: 1. Single aerosol type, *J. Geophys. Res.*, *103*, 6123–6131.

Adler, R. F., et al. (2003), The version-2 global precipitation climatology project (GPCP) monthly precipitation analysis (1979–present), *J. Hydrometeorol.*, *4*, 1147–1167.

Albrecht, B. A. (1989), Aerosols, cloud microphysics, and fractional cloudiness, *Science*, *245*, 1227–1230.

Berry, E. X. (1967), Cloud droplet growth by collection, *J. Atmos. Sci.*, *24*, 688–701.

d'Almeida, G. A., P. Koepke, and E. P. Shettle (1991), *Atmospheric Aerosols: Global Climatology and Radiative Characteristics*, 561 pp., A. Deepak, Hampton, Va.

Ghan, S. J., L. R. Leung, R. C. Easter, and A. Abdul-Razzak (1997), Prediction of cloud droplet number in a general circulation model, *J. Geophys. Res.*, *102*, 21,777–21,794.

Ghan, S. J., N. Laulainen, R. Easter, R. Wagener, S. Nemesure, E. Chapman, Y. Zhang, and R. Lenug (2001), Evaluation of aerosol direct radiative forcing in MIRAGE, *J. Geophys. Res.*, *106*, 5295–5316.

Hansen, J., et al. (2002), Climate forcings in Goddard Institute for Space Studies SI2000 simulations, *J. Geophys. Res.*, *107*(D18), 4347, doi:10.1029/2001JD001143.

Harrison, E. F., P. Minnis, B. R. Barkstrom, V. Ramanathan, R. D. Cess, and G. G. Gibson (1990), Seasonal variation of cloud radiative forcing derived from the Earth Radiation Budget Experiment, *J. Geophys. Res.*, *95*, 18,687–18,703.

Haywood, J. M., and V. Ramaswamy (1998), Global sensitivity studies of the direct radiative forcing due to anthropogenic sulfate and black carbon aerosols, *J. Geophys. Res.*, *103*, 6043–6058.

Higurashi, A., T. Nakajima, B. N. Holben, A. Smirnov, R. Frouin, and B. Chatenet (2000), A study of global aerosol optical climatology with two channel AVHRR remote sensing, *J. Clim.*, *13*, 2011–2027.

Hobbs, P. V. (2000), *Introduction to Atmospheric Chemistry*, 262 pp., Cambridge Univ. Press, New York.

Hobbs, P. V., J. S. Reid, R. A. Kotchenruther, R. J. Ferek, and R. Weiss (1997), Direct radiative forcing by smoke from biomass burning, *Science*, *275*, 1776–1778.

Holben, B. N., et al. (2001), An emerging ground-based aerosol climatology: Aerosol optical depth from AERONET, *J. Geophys. Res.*, *106*, 12,067–12,097.

Intergovernmental Panel on Climate Change (IPCC) (1996), *Climate Change 1995: The Science of Climate Change*, edited by J. T. Houghton et al., 572 pp., Cambridge Univ. Press, New York.

Intergovernmental Panel on Climate Change (IPCC) (2001), *Climate Change 2001: The Scientific Basis*, edited by J. T. Houghton et al., 896 pp., Cambridge Univ. Press, New York.

Kaufman, Y. J., D. Tanré, O. Dobocik, A. Karnieli, and L. A. Remer (2001), Absorption of sunlight by dust as inferred from satellite and ground-based remote sensing, *Geophys. Res. Lett.*, *28*, 1479–1482.

Khain, A. P., M. Ovtchinnikov, M. Pinsky, A. Pokrovsky, and H. Krugliak (2000), Note on the state-of-the-art numerical modeling of cloud microphysics, *Atmos. Res.*, *55*, 159–224.

Kinne, S., et al. (2003), Monthly averages of aerosol properties: A global comparison among models, satellite, and AERONET ground data, *J. Geophys. Res.*, *108*(D20), 4634, doi:10.1029/2001JD001253.

Lohmann, U., and B. Kärcher (2002), First interactive simulations of cirrus clouds formed by homogenous freezing in the ECHAM general circulation model, *J. Geophys. Res.*, *107*(D10), 4105, doi:10.1029/2001JD000767.

Lohmann, U., and G. Lesins (2002), Stronger constraints on the anthropogenic indirect aerosol effect, *Science*, *298*, 1012–1015.

Lohmann, U., J. Feichter, C. C. Chuang, and J. E. Penner (1999), Prediction of the number of cloud droplets in the ECHAM GCM, *J. Geophys. Res.*, *104*, 9169–9198.

Martin, G. M., D. W. Johnson, and A. Spice (1994), The measurement and parameterization of effective radius of droplets in warm stratocumulus clouds, *J. Atmos. Sci.*, *51*, 1823–1842.

Martins, J. V., P. Artaxo, P. V. Hobbs, C. Liousse, H. Cachier, Y. Kaufman, and A. Plana-Fattori (1996), Particle size distributions, elemental compositions, carbon measurements, and optical properties of smoke from biomass burning in the Pacific Northwest of the United States, in *Biomass Burning and Global Change*, vol. 2, edited by J. S. Levine, pp. 716–732, MIT Press, Cambridge, Mass.

Miller, R. L., and I. Tegen (1998), Climate response to soil dust aerosols, *J. Clim.*, *11*, 3247–3267.

Nakajima, T., M. Tsukamoto, Y. Tsushima, A. Numaguti, and T. Kimura (2000), Modeling of the radiative process in an atmospheric general circulation model, *Appl. Opt.*, *39*, 4869–4878.

Nakajima, T., A. Higurashi, K. Kawamoto, and J. E. Penner (2001), A possible correlation between satellite-derived cloud and aerosol microphysical parameters, *Geophys. Res., Lett.*, *28*, 1171–1174.

Nakajima, T. Y., and T. Nakajima (1995), Wide-area determination of cloud microphysical properties from NOAA AVHRR measurements for FIRE and ASTEX regions, *J. Atmos. Sci.*, *52*, 4043–4059.

Numaguti, A., M. Takahashi, T. Nakajima, and A. Sumi (1995), Development of an atmospheric general circulation model, in *Climate System Dynamics and Modeling*, edited by T. Matsuno, pp. 1–27, Cent. for Clim. Syst. Res., Univ. of Tokyo, Tokyo.

Peng, Y., and U. Lohmann (2003), Sensitivity study of the spectral dispersion of the cloud droplet size distribution on the indirect effect, *Geophys. Res., Lett.*, *30*(10), 1507, doi:10.1029/2003GL017192.

Rotstayn, L. D., and U. Lohmann (2002), Tropical rainfall trends and the indirect aerosol effect, *J. Clim.*, *15*, 2103–2116.

Spiro, P. A., D. J. Jacob, and J. A. Logan (1992), Global inventory of sulfur emissions with 1° × 1° resolution, *J. Geophys. Res.*, *97*, 6023–6036.

Sudo, K. M. Takahashi, J. Kurokawa, and H. Akimoto (2002), CHASER: A global chemical model of the troposphere: 1. Model description, *J. Geophys. Res.*, *107*(D17), 4339, doi:10.1029/2001JD001113.

Sundqvist, H. (1978), A parameterization scheme for non-convective condensation including prediction of cloud water content, *Q. J. R. Meteorol. Soc.*, *104*, 677–690.

Takemura, T., H. Okamoto, Y. Maruyama, A. Numaguti, A. Higurashi, and T. Nakajima (2000), Global three-dimensional simulation of aerosol optical thickness distribution of various origins, *J. Geophys. Res.*, *105*, 17,853–17,873.

Takemura, T., T. Nakajima, O. Dubovik, B. N. Holben, and S. Kinne (2002a), Single scattering albedo and radiative forcing of various aerosol species with a global three-dimensional model, *J. Clim.*, *15*, 333–352.

Takemura, T., I. Uno, T. Nakajima, A. Higurashi, and I. Sano (2002b), Modeling study of long-range transport of Asian dust and anthropogenic aerosols from east Asia, *Geophys. Res. Lett.*, *29*(24), 2158, doi:10.1029/2002GL016251.

Takemura, T., T. Nakajima, A. Higurashi, S. Ohta, and N. Sugimoto (2003), Aerosol distributions and radiative forcing over the Asian Pacific region simulated by Spectral Radiation-Transport Model for Aerosol Species (SPRINTARS), *J. Geophys. Res.*, *108*(D23), 8659, doi:10.1029/2002JD003210.

Tang, I. N., and H. R. Munkelwitz (1994), Water activities, densities, and refractive indices of aqueous sulfates and sodium nitrate droplets of atmospheric importance, *J. Geophys. Res.*, *99*, 18,801–18,808.

Twomey, S. (1974), Pollution and the planetary albedo, *Atmos. Environ.*, *8*, 1251–1256.

World Meteorological Organization (1983), Report of the experts meeting on aerosols and their climatic effects, edited by A. Deepak and H. G. Gerber, *Rep. WCP-55*, 107 pp., Geneva, Switzerland.

Zhang, Y., R. C. Easter, S. J. Ghan, and H. Abdul-Razzak (2002), Impact of aerosol size representation on modeling aerosol-cloud interactions, *J. Geophys. Res.*, *107*(D21), 4558, doi:10.1029/2001JD001549.

S. Emori and T. Nozawa, National Institute for Environmental Studies, 16-2 Onogawa, Tsukuba, Ibaraki 305-8506, Japan.

T. Nakajima, Center for Climate System Research, University of Tokyo, 4-6-1 Komaba, Meguro-ku, Tokyo 153-8904, Japan.

T. Y. Nakajima, Earth Observation Research Center, Japan Aerospace Exploration Agency, 1-8-10 Harumi, Chuo-ku, Tokyo 104-6023, Japan.

T. Takemura, Research Institute for Applied Mechanics, Kyushu University, 6-1 Kasuga-koen, Kasuga, Fukuoka 816-8580, Japan. (toshi@riam.kyushu-u.ac.jp)